Supporting Information

Achieving High Hydrogen Evolution Reaction Activity of a Mo_2C Monolayer

Huan Lou[a,b], Tong Yu[a], Jiani Ma[a], Shoutao Zhang*[a], Aitor Bergara*[c,d,e] and Guochun Yang*[a,b]

[a]Centre for Advanced Optoelectronic Functional Materials Research and Key Laboratory for UV Light-Emitting Materials and Technology of Ministry of Education, Northeast Normal University, Changchun 130024, China

[b]State Key Laboratory of Metastable Materials Science and Technology, Yanshan University, Qinhuangdao 066004, China

[c]Departamento de Física de la Materia Condensada, Universidad del País Vasco-Euskal Herriko Unibertsitatea, UPV/EHU, 48080 Bilbao, Spain

[d]Donostia International Physics Center (DIPC), 20018 Donostia, Spain

[e]Centro de Física de Materiales CFM, Centro Mixto CSIC-UPV/EHU, 20018 Donostia, Spain

*Corresponding Author Email: zhangst966@nenu.edu.cn; a.bergara@ehu.eus; yanggc468@nenu.edu.cn

Index **Page**

Computational details

1. Formation energy of vacancy defects on pritine Mo_2C monolayer

We calculate the formation energy (E_{form}), defined as

$$E_f = E_D - E_T + \Delta n_i \sum_i \mu_i \quad (1)$$

where E_D and E_T are the total energies of a Mo_2C monolayer with and without defects, respectively. μ_i is the chemical potential of atomic species i (i = Mo and C) and Δn_i is the difference of the number of Mo and C atoms between pristine and defective structures.[1,2] To maintain thermodynamic equilibrium (i.e., $\mu_{Mo_2C} = 2\mu_{Mo} + \mu_C$), the allowed range of μ_{Mo} is $\mu_{Mo(bulk)} - \Delta H_f/2 < \mu_{Mo} < \mu_{Mo(bulk)}$, where the upper (lower) limit corresponds to Mo-rich (C-rich) condition and ΔH_f is the heat of formation. Here, ΔH_f is defined as $\Delta H_f = E_{Mo_2C} - 2E_{Mo} - E_C$, where E_{Mo_2C} and $2E_{Mo}$ and E_C are the energies of the Mo_2C monolayer, Mo and C in bulk, respectively. The computed ΔH_f of 1T and 2H phases are 2.62 and 2.39 eV, respectively.

2. Adsorption sites of one hydrogen atom

For the pristine 1T- and 2H-Mo_2C monolayer, there are three different adsorption sites, i.e. S_1 sits on-top of the Mo atom, S_2 site is above the center of the hexagonal ring and S_3 sits the on-top of a C atom. After removing a C atom, there are six different adsorption sites, in addition to the above three ones, which also includes sites S_v (on-top site of a vacant atom), which is surrounded by a hexagonal ring center and two different carbon atom sites, S_4 and S_5. On the other hand, after removing a Mo atom, there are two different types of carbon atoms around a Mo vacancy, i.e. sites S_4 and S_6 (Figures S1c and d).

For the pristine 1T phase, one hydrogen atom is adsorbed on site S_1 with best ΔG_H of 0.007 eV. For VMoS-1T, the most favorable hydrogen adsorption site is S_6 with closer to 0.0 eV ΔG_H of 0.40 eV, while one hydrogen atom is adsorbed on site S_1 or S_v, and the atom moves to sites S_3 or S_6 after optimization. For PMoS-1T, the most favorable hydrogen adsorption site is S_3, with a ΔG_H of -0.40 eV. After optimization, the adsorption of hydrogen atom moves from site S_1 to S_4. For V_C-1T, the most

favorable hydrogen adsorption site is also S_3, with a ΔG_H of -0.55 eV. After optimization, the hydrogen atom cannot be stabilized at site S_1 but moves to site S_5.

For the pristine 2H phase, the hydrogen most favorable adsorption site is S_3 with a ΔG_H of -1.03 eV, while hydrogen atom does not stabilize at site S_1 but moves to S_3. As for VMoS-2H, site S_6 is relatively active for hydrogen atom adsorption with ΔG_H of 0.70 eV. After optimization, the hydrogen atom can move from site S_1 to S_2, and from site S_v to S_6. For PMoS-2H, the site S_4 is relatively active for hydrogen atom adsorption with ΔG_H of -0.79 eV. After optimization, the hydrogen atom moves from site S_1 or S_6 to S_2, and from site S_v to S_5. As for V_C, site S_3 is relatively active with ΔG_H of -1.05 eV. Among hydrogen atom cannot be stabilized on site S_1 and moves to site S_3.

3. Adsorption energy of oxygen atom on Mo_2C monolayer

In order to quantitatively access the adsorption behaviors, we debate the energetically most favorable adsorption sites of oxygen atoms on Mo_2C monolayer by calculating the adsorption energies. The adsorption energy, is defined as the difference between the total energy of the system with adsorbed oxygen atoms and the sum of the total energy of n isolated oxygen atoms and the isolated Mo_2C monolayer.[3,4] The adsorption energy (E_{ad}) is calculated as below:

$$E_{ad} = E_{O@Mo_2C} - E_{Mo_2C} - \frac{n}{2}E(O_2) \quad (5)$$

where E_{Mo_2C} and $E_{O@Mo_2C}$ represent the total energy of a Mo_2C monolayer and n O atoms adsorbed on the Mo_2C monolayer, respectively. A negative value of the adsorption energy indicates that the composite structure of the oxygen atoms adsorbed on the Mo_2C monolayer is more stable.

For 1T phase, the most favorable oxygen adsorption site is S_3 for the pristine and V_C monolayers, while site S_2 for VMoS-$V_{Mo}CO_2$-1T and PMoS-$V_{Mo}CO_2$-1T. Among the interaction between oxygen atom and the basal is weaker in the $V_{Mo}CO_2$-1T monolayer than in Mo_2CO_2-1T and V_CCO_2-1T with difference of adsorption energies of 0.47 and 0.38 eV/atom, respectively. For the 2H phase, both on the pristine and basal planes with vacancy defects, the oxygen atoms adsorbed on site S_3 is the most stable configuration. Similar to the 1T phase, the interaction between oxygen atoms and the basal plane is weaker in the $V_{Mo}CO_2$-2H monolayer than that in other basal planes with difference of adsorption energies of 0.31 and 0.27 eV/atom, respectively.

Results of the HER activity

1. Strain effect of PMoS-$V_{Mo}CO_2$-1T and V_CCO_2-1T on the HER activity

For PMoS-$V_{Mo}CO_2$-1T, d-ΔG_H values range from -0.34 to 0.10 eV at hydrogen coverages of 1/9 to 7/9, and can be tuned into the free energy range from -0.40 eV to 0.20 eV through a 4% compression and stretching (Figure 3g). Both the catalytic activity of PMoS-$V_{Mo}CO_2$-1T can be improved at a coverage of 2/9 through compressive strain from -3% to -4% with a d-ΔG_H of -0.016 and -0.0007 eV. At a coverage of 5/9, the d-ΔG_H value can be reduced to -0.01 and 0.003 eV through compression and stretching of $\pm$4%. For other hydrogen coverages, by applying strain, d-ΔG_H values decrease at θ = 1/9, 3/9 and 6/9, and increase at θ = 4/9 and 7/9, which is in the window of $\pm$0.4 eV. The range of a-ΔG_H values is from -0.09 to 0.07 eV, adjusted from -0.22 eV to 0.06 eV after applying strain, which makes a-ΔG_H more negative than without strain (Figure 3h).

For V_CCO_2-1T, by applying the appropriate strain, the d-ΔG_H values are basically unchanged at hydrogen coverages from 1/9 to 3/9, with d-ΔG_H values from -0.40 to 0.30 eV (Figure 3i). When the suitable strain is applied, the values of d-ΔG_H with coverages of 2/9 and 3/9 are closer to 0.0 eV, especially with a strain of $\pm$4% at a coverage of 2/9 with 0.03 eV. d-ΔG_H values are slightly reduced at θ = 3/9 through 4% compression and stretching. At a 5/9 coverage, the d-ΔG_H can reduce to 0.38 and 0.44 eV under compression and stretching of $\pm$4%, respectively, while the HER activity cannot be improved at θ = 1/9 and 4/9 under 4% compression and stretching. For the average process, the strain effect on a-ΔG_H value is small (ranging from -0.13 to 0.24 eV without strain and from -0.17 to 0.24 eV upon strain (Figure 3j).

2. The HER activity of the pristine and defective 2H-Mo_2C monolayer

The HER activity of catalyst is closely related to the reaction Gibbs free energy of hydrogen adsorption (ΔG_H), and the ideal ΔG_H value is close to zero, and defined as the H* adsorption sites with $|\Delta G_H| < 0.40$ eV.[5] Meanwhile, ΔG_H is closely correlated

with hydrogen coverages.[6–8] Similar to the 1T structure, the 2H phase of a Mo_2C monolayer has three inequivalent adsorption sites (Figure 1) for H atoms. In more detail, S_1 sits on-top of a Mo atom, S_2 is above the center of the hexagonal ring, and S_3 sits on-top of a C atom. There are two stable H adsorption sites after optimization, such as sites S_2 and S_3 (Figure 1b), and site S_3 is relatively active with a ΔG_H of -1.03 eV (Table S1).

Then, we calculate the average process (a-ΔG_H) and individual process (d-ΔG_H) with hydrogen coverages (θ) ranging from 1/9 to 4/9, as shown in Figures 4a and b. In the individual process, the best d-ΔG_H value is -0.73 eV at a hydrogen coverage of 4/9. With increasing the hydrogen coverage, d-ΔG_H values gradually increase, but still are more negative. In the collective process, the best a-ΔG_H value is -0.86 eV at a hydrogen coverage of 4/9. a-ΔG_H values gradually increase by increasing the hydrogen coverage, similar to the d-ΔG_H. Thus, d-ΔG_H and a-ΔG_H values are out of the window of $\pm$0.40 eV, though the 2H phase is more energetically stable, it has a poor HER activity, as demonstrated in previous study.[9]

Subsequently, we explore the effect of Mo and C vacancy on the HER activity of the 2H phase. As observed in the 1T phase, there are two independent surfaces (i.e. VMoS-2H and PMoS-2H). For VMoS-2H, five possible adsorption sites for hydrogen atoms are considered (Figure 1d, Figure S4d, and Table S1). Its most favorable hydrogen adsorption site is on the C atom (S_6 site), similar to VMoS-1T. The Gibbs free energy related to hydrogen coverages (θ) ranging from 1/9 to 4/9 are listed in Table S4. As shown in Figures 4a and b, the best d-ΔG_H and a-ΔG_H values are -0.42 and -0.64 eV, respectively, at a hydrogen coverage of 4/9. Both d-ΔG_H and a-ΔG_H values are far from the accepted window of $\pm$0.40 eV. Compared with pristine 2H-Mo_2C, the incorporation of Mo vacancy strengthens the HER activity, which may be due to the appearance of dangling bonds.

For PMoS-2H, all possible adsorption sites of hydrogen atoms are considered (Figure 1d, Figure S4f, and Table S1). The most favorable hydrogen adsorption site is on the C atom (S_4 site). The calculated Gibbs free energy of hydrogen adsorption with coverages (θ) from 1/9 to 4/9 can be found in Table S4. In the individual process (Figure 4a), the best d-ΔG_H is -0.18 eV at a hydrogen coverage of 2/9, indicating a

good HER activity on PMoS-2H. At other hydrogen coverages, d-ΔG_H values are outside the energy window of $\pm$0.40 eV. In the average process (Figure 4b), the best a-ΔG_H value is -0.49 eV at a hydrogen coverage of 2/9. Based on the analysis above, the HER activity of the individual process is superior to that of the average process. Compared with VMoS-2H, PMoS-2H shows a better HER activity in the individual and collective processes.

Five possible adsorption sites for hydrogen atoms are also considered for V_C (Figure 1f, Figure S4h, and Table S1). We calculate d-ΔG_H and a-ΔG_H with hydrogen coverages (θ) ranging from 1/9 to 4/9 (Figure S10c and Table S4). In the individual process (Figure 4a), the best d-ΔG_H value is -0.60 eV at a hydrogen coverage of 4/9. a-ΔG_H values at hydrogen coverages from 1/9 to 4/9 are less than -1.00 eV (Figure 4b). Thus, the incorporation of C vacancies does not improve the HER activity of the 2H phase.

3. The HER activity of 2H-Mo_2C monolayer with oxygen functionalization

The HER activity of the pristine and defective 2H-Mo_2C with oxygen functionalization were considered (Figure S11), which is named as Mo_2CO_2-2H, VMoS-$V_{Mo}CO_2$-2H, PMoS-$V_{Mo}CO_2$-2H, and V_CCO_2-2H. For 2H-Mo_2C, similar to the 1T phase, there are also three possible adsorption sites for oxygen atoms (i.e. sites S_1, S_2, and S_3, Figure 1b). After fully relaxed the structure, the most favorable O adsorption site both for pristine and for the basal planes of the 2H phase with vacancy defects is S_3.

For Mo_2CO_2-2H, we calculated the d-ΔG_H and a-ΔG_H with hydrogen coverages (θ) ranging from 1/9 to 5/9 (Table S5). In the individual process (Figures 4c), the best d-ΔG_H is 0.06 eV at a hydrogen coverage of 2/9. With increasing hydrogen coverages, the interaction between hydrogen atoms and Mo_2CO_2-2H becomes weaker with d-ΔG_H ranging from -0.48 to 1.67 eV, which is out of the accepted window of $\pm$0.40 eV. In the average process (Figures 4d), the best a-ΔG_H is 0.11 eV at a hydrogen coverage of 3/9. With increasing hydrogen coverages, the interaction between hydrogen atoms and Mo_2CO_2-2H also becomes weaker with a a-ΔG_H ranging from -0.21 to 0.73 eV at θ = 2/9, 3/9, 4/9 and 5/9. The resulting catalytic activity of the 2H phase is enhanced by oxygen functionalization.

For VMoS-$V_{Mo}CO_2$-2H, the maximum absorbed hydrogen has been greatly enhanced, and hydrogen coverages (θ) ranging from 1/9 to 9/9 are studied (Figure S11b and Table S5). In the individual process (Figure S12a), there appear more ideal Gibbs free energy values of hydrogen adsorption (i.e. -0.19, -0.15, 0.18, 0.005, 0.24, -0.05 and 0.22 eV at θ = 1/9, 2/9, 3/9, 4/9, 5/9, 6/9, and 7/9, respectively), indicating VMoS-$V_{Mo}CO_2$-2H possesses an excellent HER activity in a wide H coverage. In the average process (Figure S12b), the best a-ΔG_H is 0.0 eV at a hydrogen coverage of 6/9. The values of a-ΔG_H range from -0.17 to 0.19 eV at hydrogen coverages from 2/9 to 8/9, and a-ΔG_H values reach to 0.43 eV at a fully hydrogen coverage. Therefore, VMoS-$V_{Mo}CO_2$-2H exhibits an excellent HER activity in both individual and collective processes, and is much superior to pristine and defective 2H-Mo_2C.

For PMoS-$V_{Mo}CO_2$-2H, d-ΔG_H and a-ΔG_H values are calculated with hydrogen coverages (θ) of 1/9 to 5/9 (Figure S11d and Table S5). In the individual process (Figure 4c), the best d-ΔG_H is 0.18 eV at a hydrogen coverage of 2/9. With increasing hydrogen coverages, the interaction between hydrogen atom and PMoS-$V_{Mo}CO_2$-2H becomes weaker, with d-ΔG_H ranging from -0.32 to 1.09 eV, which is out of the accepted window of $\pm$0.40 eV. In the average process (Figures 4d), the best a-ΔG_H is 0.04 eV at a hydrogen coverage of 3/9. With increasing hydrogen coverages, the interaction between hydrogen atoms and PMoS-$V_{Mo}CO_2$-2H also becomes weaker with a-ΔG_H changing from -0.07 to 0.41 eV at θ = 2/9 to 5/9. Thus, PMoS-$V_{Mo}CO_2$-2H shows an excellent HER activity in the collective process. Therefore, incorporation of Mo vacancies and oxygen functionalization are the effective way to enhance the HER activity of 2H-Mo_2C, and VMoS-$V_{Mo}CO_2$-2H shows an excellent HER activity both in the individual and collective processes with a wide hydrogen coverage.

For V_CCO_2-2H, we investigated the corresponding d-ΔG_H and a-ΔG_H at different hydrogen coverages (θ) from 1/9 to 5/9 (Figure S11c and Table S5). In the individual process (Figure 4c), the d-ΔG_H values are -0.34, 0.05, 0.26 and -0.13 eV at θ = 1/9, 2/9, 3/9, and 4/9, respectively, indicating that V_CCO_2-2H has a good HER activity. In the average process (Figure 4d), the a-ΔG_H values are -0.14, -0.009, -0.04 and -0.23 eV at θ = 2/9, 3/9, 4/9, and 5/9, respectively, indicating that V_CCO_2-2H shows an improved HER activity with respect to V_C-2H. In other words, oxygen functionalization is able to enhance the HER activity of 2H-Mo_2C with C vacancies.

However, the HER activity of V_CCO_2-2H is much weaker than that of VMoS-$V_{Mo}CO_2$-2H.

Supporting Figures

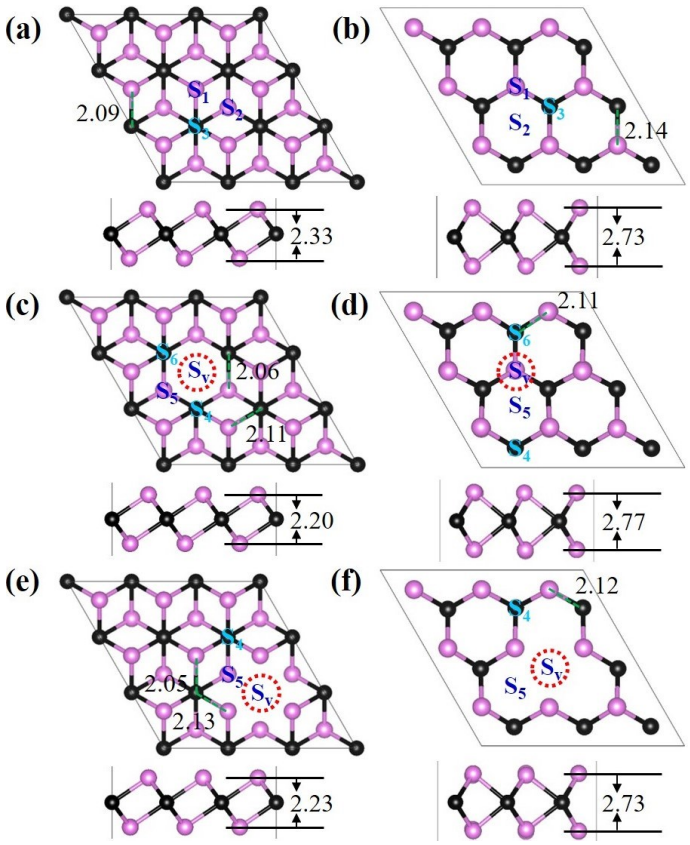

Figure S1. The optimized structures and the potential adsorption sites of the pristine and vacancy defects of 1T and 2H phases of Mo_2C. (a) and (b) are the pristine structures of 1T and 2H phases. (c) and (d) are the structures with V_{Mo}. (e) and (f) are for V_C ones. Light violet and black balls represent Mo and C atoms, respectively. Sites S_1, S_2 and S_3 are located on-top of a Mo atom, the center of the hexagonal ring and on-top of a C atom, respectively. The defect site is denoted as S_v, which is surrounded by a hexagonal ring center and two different carbon atom sites, S_4 and S_5.

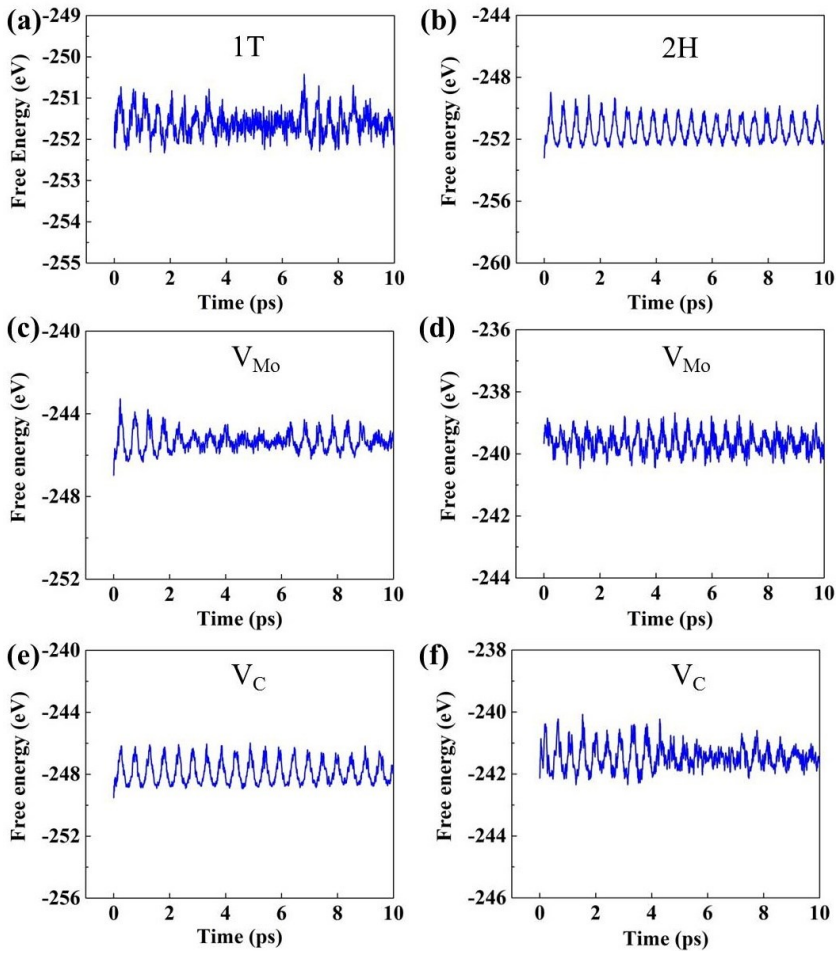

Figure S2. Total potential energy as a function of MD time at a temperature of 500 K.

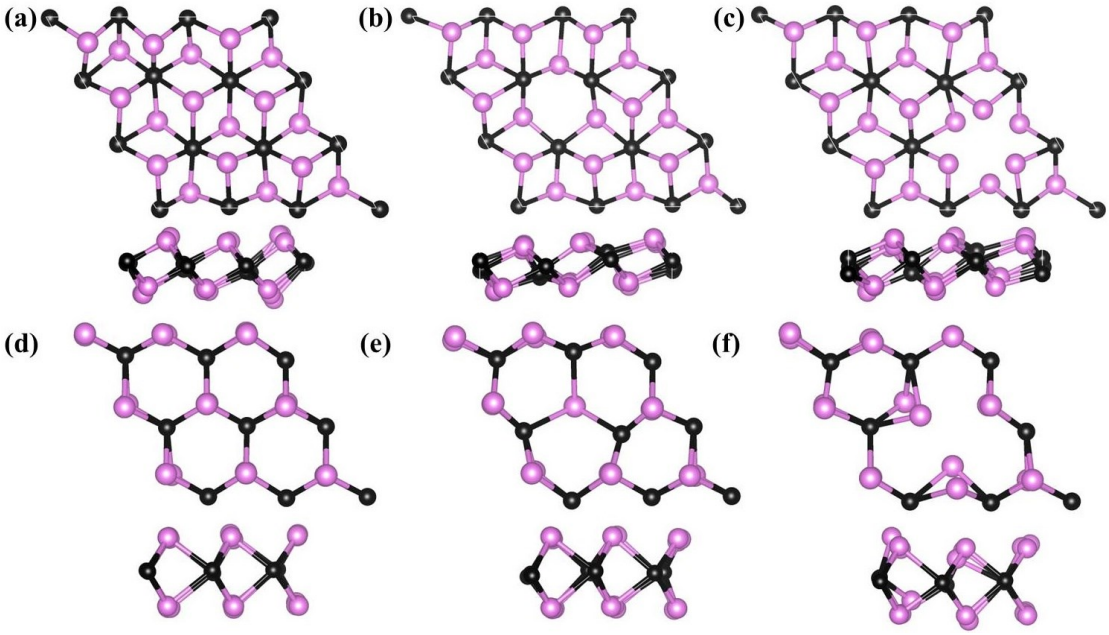

Figure S3. Snapshots of the final frame of Mo_2C monolayers at time of 10 ps during AIMD simulations under the temperatures of 500 K, (a-c)pristine, V_{Mo} and V_C of 1T phase, respectively, (d-f) pristine, V_{Mo} and V_C of 2H phase, respectively.

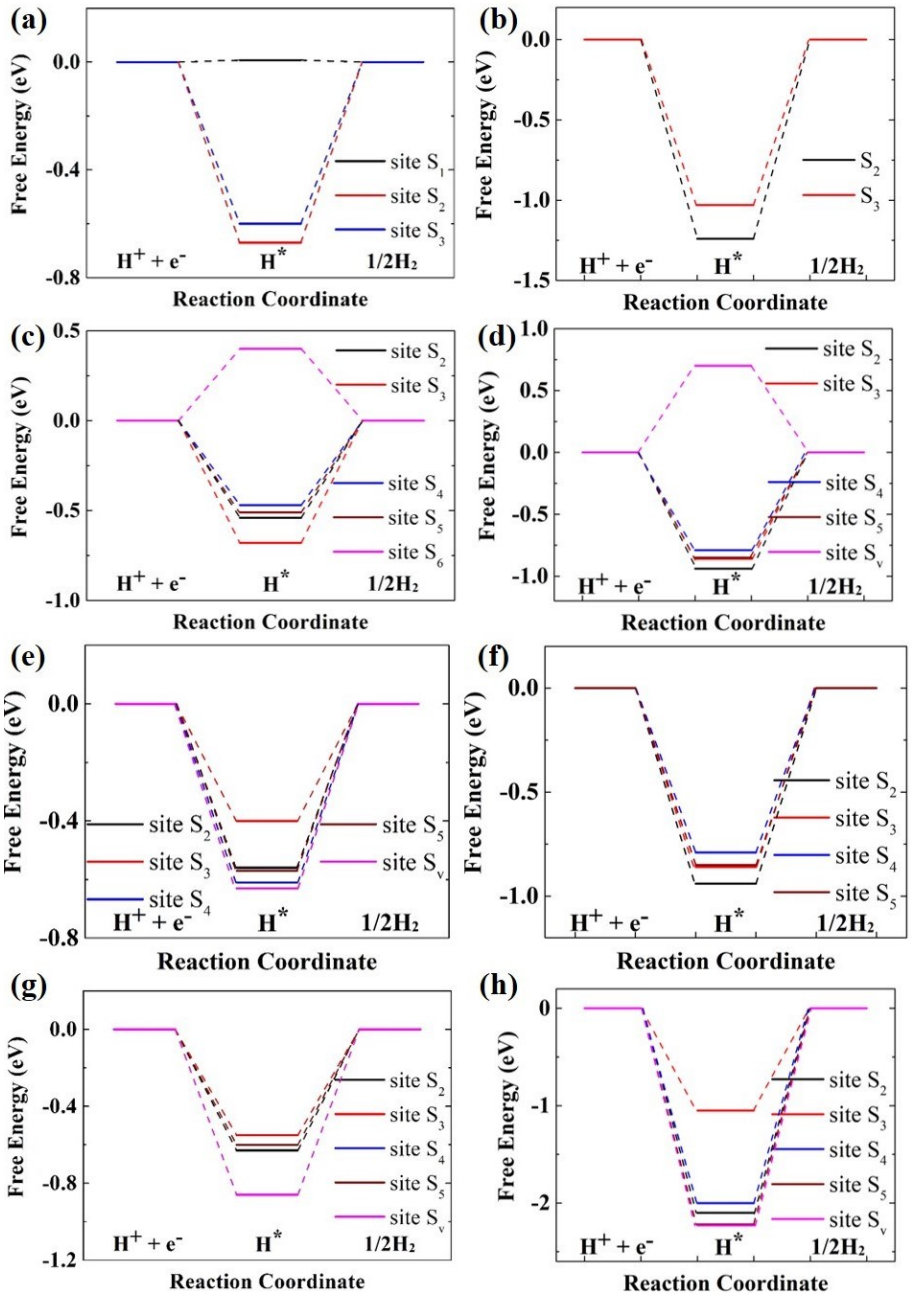

Figure S4. Calculated Gibbs free energies of different adsorption sites on the pristine and vacancy defect of 1T- (left) and 2H- (right) Mo_2C monolayers with vacancy defects: (a, b) pristine, (c, d) VMoS, (e, f) PMoS, and (g, h) V_C. For PMoS of 1T phase, it only shows the free energy of site S_4 because hydrogen atoms adsorbed on sites S_4 and S_6 have the same value of ΔG_H.

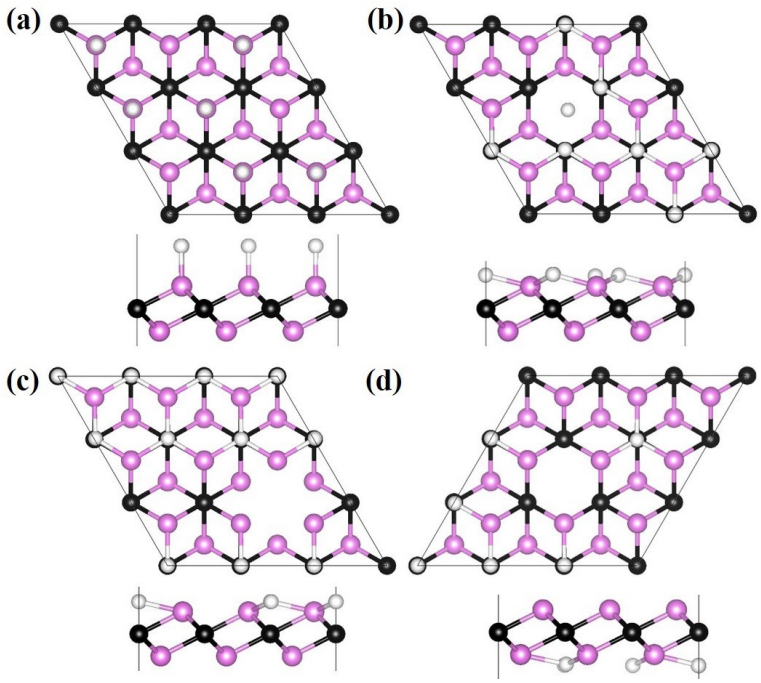

Figure S5. Optimized structures on pristine and vacancy defects of 1T-Mo_2C monolayer with H coverage, (a) pristine, (b) VMoS-1T, (c) V_C and (d) PMoST-1T. Light purple, black and light grey balls represent Mo, C and H atoms, respectively.

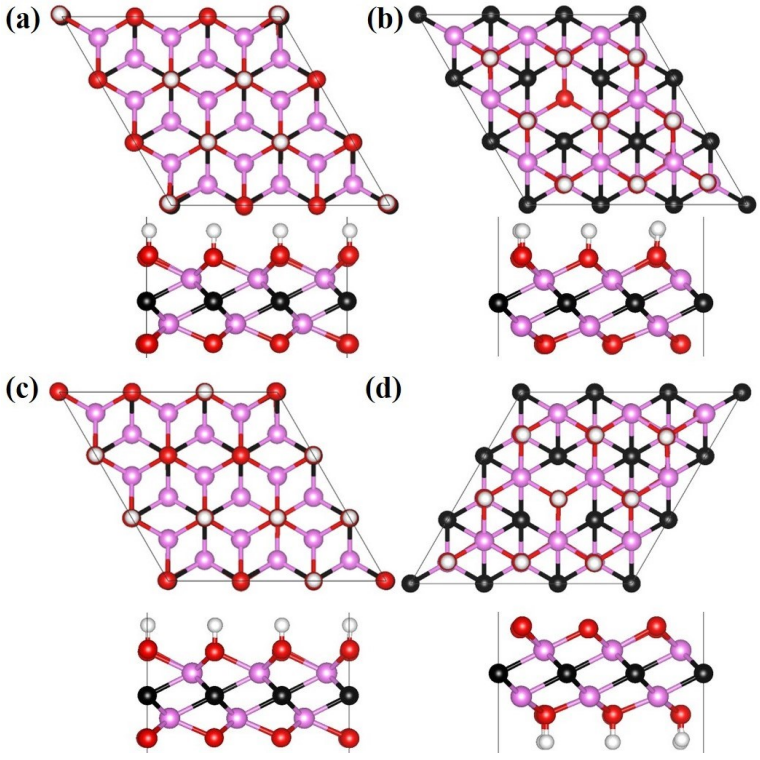

Figure S6. Optimized structures of pristine and oxygen-terminated 1T-Mo_2C monolayer with vacancy defects and H coverage: (a) pristine, (b) VMoST-1T, (c) V_C and (d) PMoST-1T. Light purple, black, red and light grey balls represent Mo, C, O and H atoms, respectively.

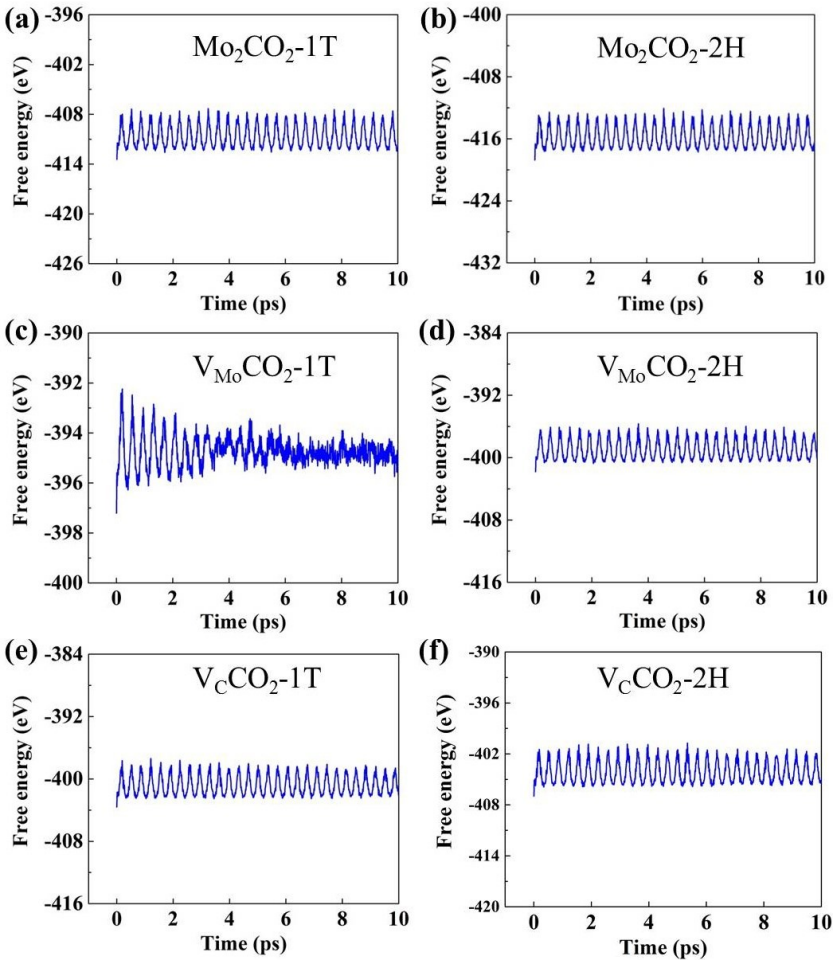

Figure S7. Total potential energy as a function of MD time at a temperature of 500 K.

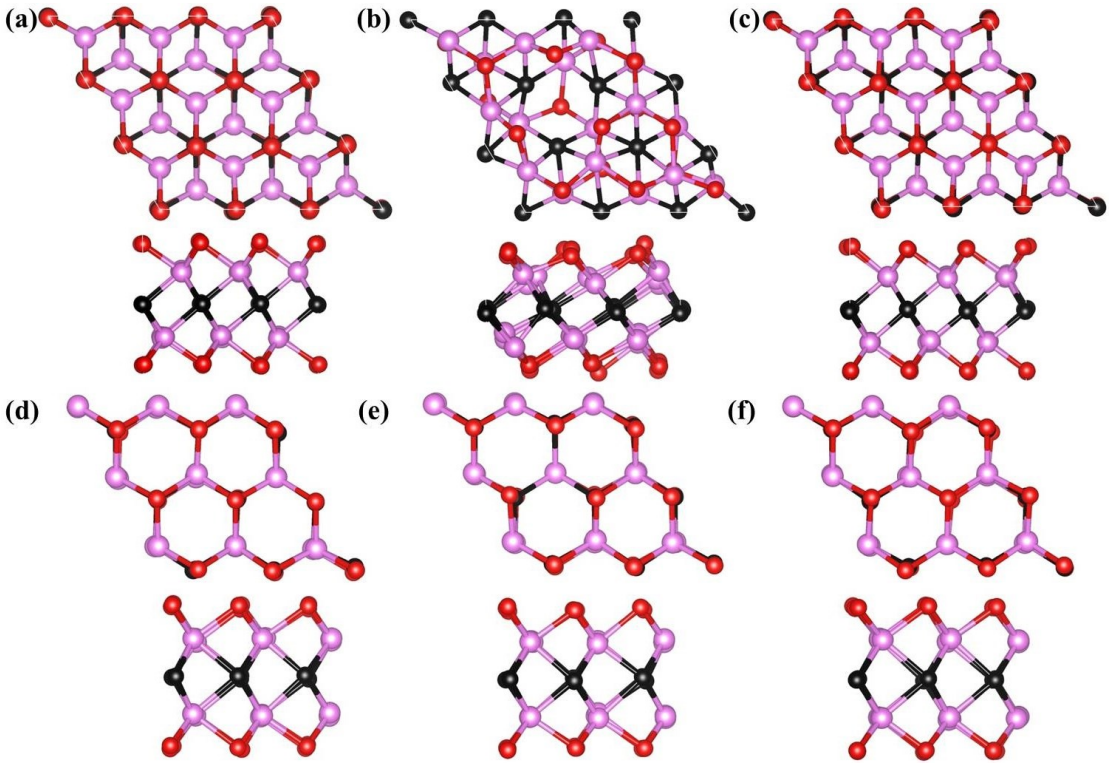

Figure S8. Snapshots of the final frame of Mo_2C monolayers with oxygen functionalization at time of 10 ps during AIMD simulations under the temperatures of 500 K, (a)Mo_2CO_2-1T, (b)$V_{Mo}CO_2$-1T, (c)V_CCO_2-1T, (d)Mo_2CO_2-2H, (e)$V_{Mo}CO_2$-2H, (f)V_CCO_2-2H.

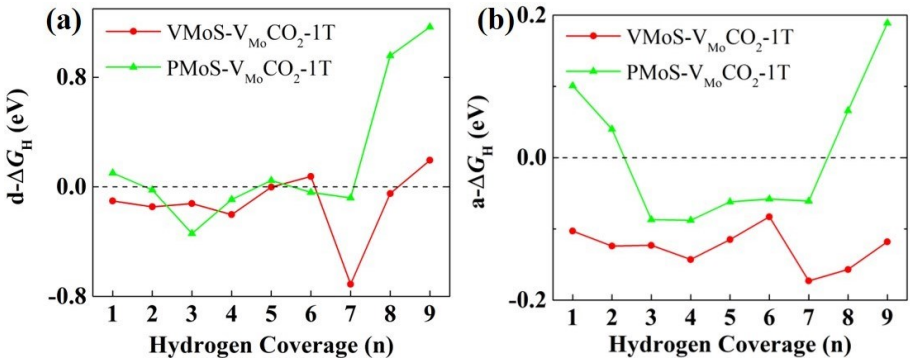

Figure S9. Calculated differential Gibbs free energies as a function of H coverage of Mo defective 1T-Mo_2C with oxygen functionalization: (a) d-$^{\Delta G_H}$ and (b) a-$^{\Delta G_H}$.

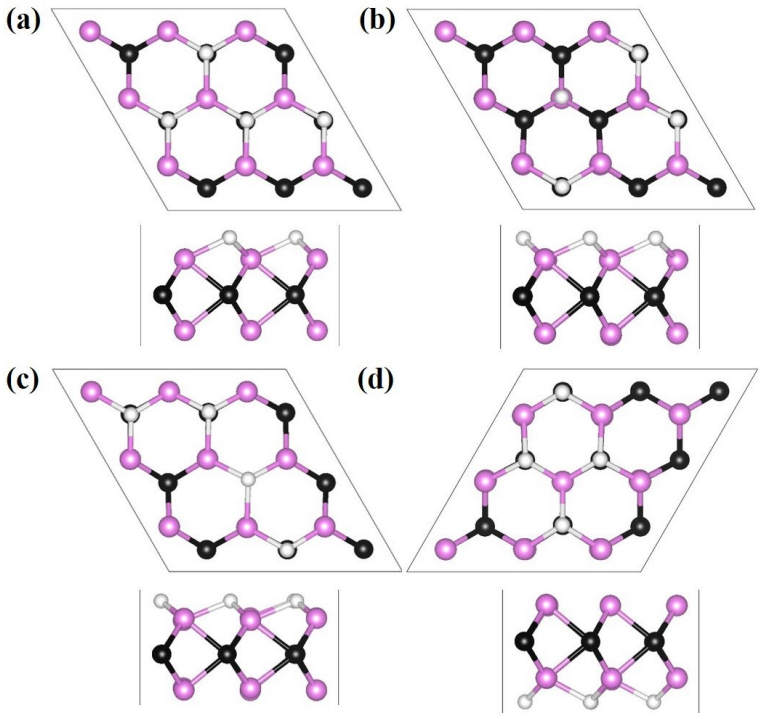

Figure S10. Optimized structures on pristine and vacancy defects of a 2H-Mo_2C monolayer with H coverage, (a) pristine, (b) VMoS-2H, (c) V_C and (d) PMoS-2H. Light purple, black and light grey balls represent Mo, C and H atoms, respectively.

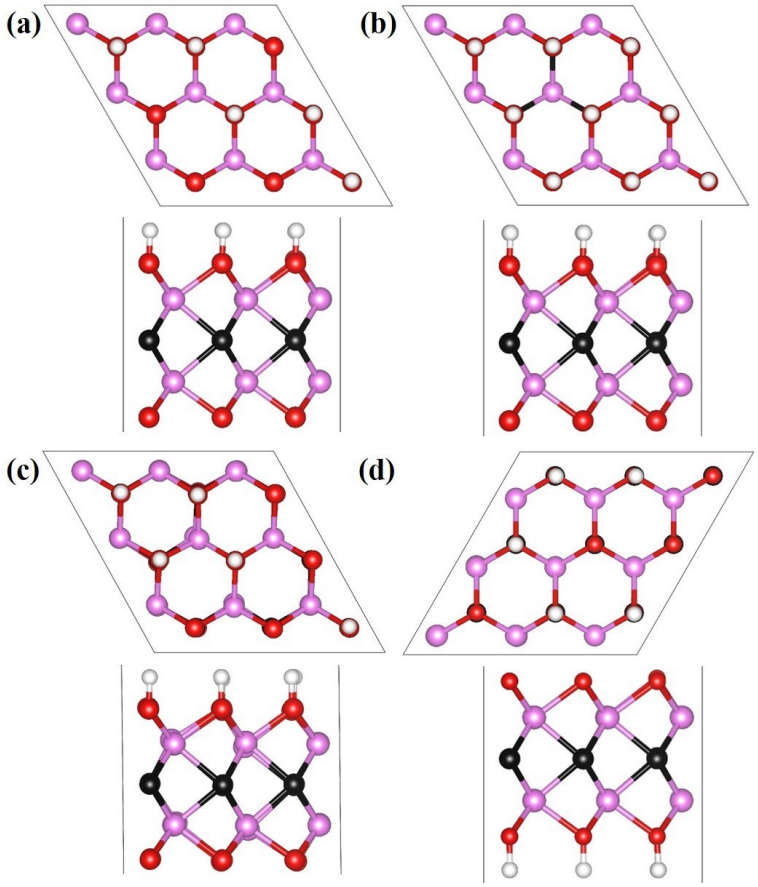

Figure S11. Optimized structures on pristine and vacancy defects of oxygen-terminated 2H-Mo_2C monolayer with H coverage, (a) pristine, (b) VMoS-2H, (c) V_C and (d) PMoS-2H. Light purple, black, red and light grey balls represent Mo, C, O and H atoms, respectively.

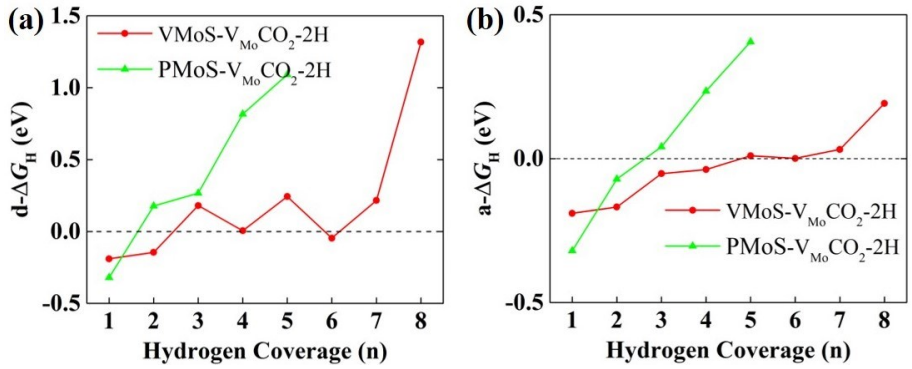

Figure S12. Calculated differential Gibbs free energies as a function of H coverage of Mo defective 2H-Mo_2C with oxygen functionalization: (a) d-$^{\Delta G_H}$ and (b) a-$^{\Delta G_H}$.

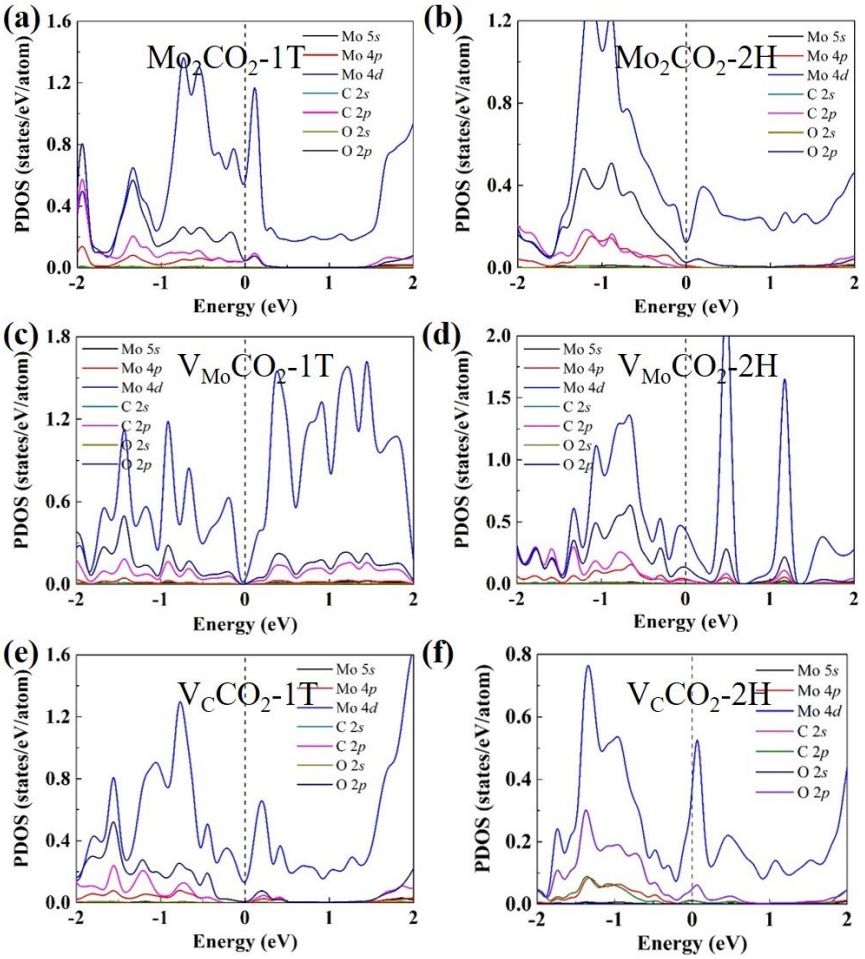

Figure S13. The projected density of states (PDOS) of the pristine and the 2H-Mo_2C monolayer with vacancy defects and oxygen functionalization.

Supporting Tables

Table S1. Calculated Gibbs free energies of different adsorption sites on the pristine and vacancy defects of 1T- and 2H-Mo_2C monolayers.

	1T phase				2H phase			
site	**Pristine**	**VMoS**	**PMoS**	**V_C**	**Pristine**	**VMoS**	**PMoS**	**V_C**
S_1	0.007							
S_2	-0.67	-0.54	-0.56	-0.63	-1.24	-0.94	-0.94	-2.10
S_3	-0.60	-0.68	-0.40	-0.55	-1.03	-0.86	-0.85	-1.05
S_4		-0.47	-0.61	-0.60		-0.79	-0.79	-2.00
S_5		-0.51	-0.57	-0.60		-0.85	-0.85	-2.22
S_6		0.40	-0.61			0.70		
S_v			-0.63	-0.86				-2.22

Table S2. Calculated d-ΔG_H and a-ΔG_H (eV), respectively, for different H atoms (n) adsorbed on the 1T-Mo_2C monolayer.

	1T phase							
n	**Pristine**		**VMoS**		**PMoS**		**V_C**	
1	0.007	0.007	0.40	0.40	-0.40	-0.40	-0.55	-0.55
2	0.01	0.01	-0.59	-0.09	-0.32	-0.36	-0.48	-0.52
3	-0.02	0.002	-0.40	-0.19	-0.23	-0.32	-0.47	-0.50
4	-1.98	-0.49	-0.49	-0.27	-0.55	-0.37	-0.44	-0.49
5	0.04	-0.39	-0.30	-0.27	-0.51	-0.40	-0.52	-0.49
6	-1.55	0.02	-0.47	-0.31	-0.44	-0.41	-0.42	-0.48

Table S3. Calculated d-ΔG_H and a-ΔG_H (eV), respectively, for different H atoms (n) adsorbed on the oxygen-terminated 1T-Mo_2C monolayer.

	1T phase							
n	**Pristine**		**VMoS**		**PMoS**		**V_C**	
1	-0.69	-0.69	-0.10	-0.10	0.10	0.10	-0.33	-0.33
2	0.01	-0.34	-0.15	-0.12	-0.02	0.04	0.06	-0.13
3	0.08	-0.20	-0.12	-0.12	-0.34	-0.09	0.29	0.008
4	0.87	0.07	-0.20	-0.14	0.09	-0.09	0.47	0.12

5	1.63	0.38	-0.002	-0.12	0.05	-0.06	0.71	0.24
6			0.08	-0.08	-0.04	-0.06		
7			-0.71	-0.17	-0.08	-0.06		
8			-0.05	-0.16	0.96	0.07		
9			0.19	-0.12	1.17	0.19		

Table S4. Calculated d-ΔG_H and a-ΔG_H (eV), respectively, for different H atoms (n) adsorbed on a 2H-Mo_2C monolayer.

2H phase								
n	**Pristine**		**VMoS**		**PMoS**		**V_C**	
1	-1.03	-1.03	0.70	0.70	-0.79	-0.79	-1.05	-1.05
2	-0.90	-0.97	-2.38	-0.84	-0.18	-0.49	-0.97	-1.01
3	-0.77	-0.90	-0.46	-0.72	-0.65	-0.54	-1.66	-1.23
4	-0.73	-0.86	-0.42	-0.64	-0.58	-0.55	-0.60	-1.07

Table S5. Calculated d-ΔG_H and a-ΔG_H (eV), respectively, for different H atoms (n) adsorbed on an oxygen-terminated 2H-Mo_2C monolayer.

2H phase								
n	**Pristine**		**VMoS**		**PMoS**		**V_C**	
1	-0.48	-0.48	-0.19	-0.19	-0.32	-0.32	-0.34	-0.34
2	0.06	-0.21	-0.15	-0.17	0.18	-0.07	0.05	-0.14
3	0.75	0.11	0.18	-0.05	0.27	0.04	0.26	-0.009
4	1.63	0.49	0.005	-0.04	0.82	0.24	-0.13	-0.04
5	1.67	0.73	0.24	0.01	1.09	0.41	1.32	0.23
6			-0.05	0.0008				
7			0.22	0.03				
8			1.32	0.19				
9			2.30	0.43				

References

1 H. Shu, D. Zhou, F. Li, D. Cao and X. Chen, Defect Engineering in $MoSe_2$ for the Hydrogen Evolution Reaction: From Point Defects to Edges, *ACS App. Mater. Inter.*, 2017, **9**, 42688–42698.

2 Y. Zhang, X. Chen, Y. Huang, C. Zhang, F. Li and H. Shu, The Role of Intrinsic Defects in Electrocatalytic Activity of Monolayer VS_2 Basal Planes for the Hydrogen Evolution Reaction, *J. Phys. Chem. C*, 2017, **121**, 1530–1536.

3 Q. Sun, Y. Dai, Y. Ma, W. Wei and B. Huang, Vertical and Bidirectional Heterostructures from Graphyne and MSe_2 (M = Mo, W), *J. Phys. Chem. Lett.*, 2015, **6**, 2694–2701.

4 Q. Sun, Y. Dai, Y. Ma, T. Jing, W. Wei and B. Huang, Ab Initio Prediction and Characterization of Mo_2C Monolayer as Anodes for Lithium-Ion and Sodium-Ion Batteries, *J. Phys. Chem. Lett.*, 2016, **7**, 937–943.

5 D. A. Kuznetsov, Z. Chen, P. V. Kumar, A. Tsoukalou, A. Kierzkowska, P. M. Abdala, O. V. Safonova, A. Fedorov and C. R. Müller, Single Site Cobalt Substitution in 2D Molybdenum Carbide (MXene) Enhances Catalytic Activity in the Hydrogen Evolution Reaction, *J. Am. Chem. Soc.*, 2019, **141**, 17809–17816.

6 Q. Tang and D. E. Jiang, Mechanism of Hydrogen Evolution Reaction on 1T-MoS_2 from First Principles, *ACS Catal.*, 2016, **6**, 4953–4961.

7 Y. Shao, M. Shao, Y. Kawazoe, X. Shi and H. Pan, Exploring New Two-Dimensional Monolayers: Pentagonal Transition Metal Borides/Carbides (Penta-TMB/Cs), *J. Mater. Chem. A*, 2018, **6**, 10226–10232.

8 H. Wu, X. Li, R. Zhang and J. Yang, Proposal of a Stable B_3S Nanosheet as an Efficient Hydrogen Evolution Catalyst, *J. Mater. Chem. A*, 2019, **7**, 3752–3756.

9 X. Lv, W. Wei, P. Zhao, D. Er, B. Huang, Y. Dai and T. Jacob, Oxygen-Terminated BiXenes and Derived Single Atom Catalysts for the Hydrogen Evolution Reaction, *J. Catal.*, 2019, **378**, 97–103.